

In situ synthesis of Cu (ii) dicarboxylate metal organic frameworks (MOFs) and their application as battery materials

Matthew Teusner^a, Jitendra Mata^b and Neeraj Sharma ^{*a}

^a*School of Chemistry, The University of New South Wales (UNSW Sydney), Sydney NSW 2052, Australia.*

^b*Australian Centre for Neutron Scattering (ACNS), Australian Nuclear Science and Technology Organisation (ANSTO), New Illawarra Rd, Lucas Heights NSW 2234, Australia.*

Supporting information

Experimental

To make the acid electrodes, a slurry was prepared using a 5:4:1 ratio of the acids (Sigma-Aldrich, 99.9%), conductive carbon black and polyvinylidene difluoride (PVDF) binder in N-methyl pyrrolidone (NMP) which was magnetically stirred overnight. The slurry was spread onto a copper or aluminium foil current collector at 100 μm thickness using a notch bar, resulting in an active material loading of approximately 0.8 – 1.2 mgcm^{-2} . The electrode sheets were dried overnight in a vacuum oven at 70 $^{\circ}\text{C}$ under a static vacuum of 0.06 MPa. The copper electrodes were dried further at 100 $^{\circ}\text{C}$ under dynamic vacuum overnight to ensure removal of residual NMP. This second drying step was not possible for the aluminium electrodes due to the sublimation of some of the acids (detailed in the results and discussion). After drying, the electrodes were pressed for an hour at 100 kNm^{-2} using a flat plate press (MTI corporation) to ensure good contact between the anode mixture and the substrate. For the creation of coin cells, 12 mm anode discs were punched from the electrode sheet and dried for an hour at 100 $^{\circ}\text{C}$ under dynamic vacuum to remove any residual moisture before transferring into

an Ar-filled glovebox for cell assembly. CR2032 coin cells were assembled, with a glass-fibre separator soaked in electrolyte, and Li used as the counter electrode. The electrolyte used was 1 M LiPF₆ in 1:1 ethylene carbonate (EC)/dimethyl carbonate (DMC).

For the galvanostatic cycling tests, the coin cells were discharged and charged at 50 mA g⁻¹ between 0.01-3 V using a cell cycler system (Neware BTS3000 or LANDT BTS CT3002A). For the rate capability tests, the MAL cells were pre-cycled 20 times at 50 mA g⁻¹ between 0.01-3 V, to minimise the effect of the capacity increase over the initial cycles, and the ASP cells were pre-cycled twice at 50 mA g⁻¹ to allow formation of the SEI. Subsequent sets of 5 cycles were performed at 69, 138, 276, 552, 1104 and finally 17 mA g⁻¹. CB electrode data is the same data that was published in our previous paper²⁵.

For scanning electron microscopy (SEM), the samples were coated with platinum for 30 s using a quorum sputter coater (sc7620). They were imaged using a Hitachi TM4000 at 5 or 15 kV. For the cycled electrode SEM, coin cells were cycled a number of times as stated, at 50 mA h g⁻¹, before discharge to 0.01 V or charge to 3 V. The cells were then disassembled in the glove box, and the anode was washed with DMC and left to dry before being analysed. X-ray diffraction (XRD) data were collected using a PANalytical Xpert Multipurpose X-ray Diffraction System at the Mark Wainwright Analytical Centre, UNSW. The instrument was operated at a voltage of 45 kV and current of 40 mA, employing Cu K α ($\lambda = 1.54 \text{ \AA}$) radiation with step size of 0.013 ° in the range $10 < 2\theta < 55$. XRD data were collected on the powders and processed electrodes.

Acid samples for nuclear magnetic resonance (NMR) spectroscopy were prepared by dissolving ~ 10 mg of the acid in 1 mL D₂O. Electrode Samples for nuclear magnetic resonance (NMR) spectroscopy were prepared by taking ~100 mg of the pristine electrode and cutting it into small pieces which were placed in ~ 1.5 mL of D₂O. The suspended electrode pieces were mechanically agitated with a spatula and sonication for 10 minutes, followed by being left to sit for 1 hour. The suspension was filtered and 1 mL of the filtrate was taken for measurement. NMR spectroscopy was

performed using a Bruker Avance III HD 400 spectrometer (^1H 300.13 MHz, ^{13}C 100.622 MHz), with a 5 mm BBFO+ probe. For the ^1H the spectrometer parameters were: 6393.862 Hz sweep width, 2.56 s acquisition time and 5 s recycle delay. Samples were analysed in D_2O . All chemical shifts are stated in ppm (δ) relative to tetramethylsilane ($\delta = 0$ ppm), referenced to the chemical shifts of residual solvent resonances (^1H). For the ^{13}C the spectrometer parameters were: 24038.461 Hz sweep width, 1.36 s acquisition time and 1 s recycle delay. Samples were analysed in D_2O . NMR spectra were processed using the Bruker TOPSPIN 3.0 software, and figures were generated using MestReNova.

Small angle neutron scattering (SANS) measurements were carried out on Quokka²⁶, while ultra-small angle neutron scattering (USANS) measurements were carried out on Kookaburra²⁷ both at the Australian Nuclear Science and Technology Organisation (ANSTO), Lucas Heights, Australia. 100 μm electrodes were prepared on copper and aluminium foil (using the previously mentioned method) and the samples were mounted on the front face of sample holder. Sample thickness (copper + electrode) was taken as 100 μm for the purposes of intensity scaling. SANS scattering data were radially averaged (under the assumption of isotropic scattering) and placed on an absolute scale using the direct beam intensity. Data were plotted I vs q in which the value of q was defined as:

$$q = \frac{4\pi\sin\theta}{\lambda}$$

where λ is the wavelength of the incident neutron beam and 2θ is the angle of scattering. For SANS, neutrons with wavelengths of 5 and 8.1 \AA were used and data were collected on two-dimensional detectors positioned at 1.3 (with 300 mm offset), 12 and 20 (lens optic with 8.1 \AA) m from the sample. For USANS, neutrons with a wavelength of 4.74 \AA were used. USANS data were converted to absolute scale and then de-smearred to combine with SANS data. The SANS and USANS data were combined using Igor Pro, and the data for the carbon electrode was multiplied 4/9 to account for the carbon black ratio in the acid electrodes. Due to the broadening of the Guinier regions²⁸ caused by polydispersity, Kratky curves (q^2I vs. q) were generated to help emphasise the q -range of the observed scattering objects. The q -range was estimated by fitting Gaussians to the Kratky plots using Igor Pro,

as the peak maximum corresponds to the relative length scale of the scattering objects. The data was fitted using the SASview software (<http://www.sasview.org/>). The scattering intensity from the samples were fitted with a combined Guinier-Porod and Power law model, which are described by the below equations. The Guinier-Porod model is composed of two contributions²⁸⁻²⁹:

$$I(Q) = \frac{G}{Q^s} \exp\left(\frac{-Q^2 R_g^2}{3-s}\right), \text{ for } q \leq q_1$$

$$I(Q) = \frac{D}{Q^m}, \text{ for } q \geq q_1$$

Where Q is the scattering variable, I(Q) is the scattering intensity, R_g is the radius of gyration, s is the dimension variable, m is the Porod exponent, and G and D are the Guinier and Porod scale factors, respectively. See ²⁸ for full derivation. The Power law model is defined as³⁰:

$$I(Q) = S q^{-x} + \text{background}$$

Where I(Q) is the scattering intensity, S is the scaling factor, q is the scattering variable and x is the Power law exponent.

Accounting for carbon black in the capacity calculations

Methodology was conducted as previously reported, using the same data¹.

Specifically:

Due to the high percentage of carbon black (CB) in the electrodes, a 9:1 CB:PVDF electrode was used as a control to isolate and understand the contribution of both the CB and the active components of the electrodes. The reversible capacity of the CB electrode after the first 100 cycles was 192 mAhg⁻¹ (Figure S9a). The capacity retention of the CB electrode was ~100% over 100 cycles, suggesting that any capacity loss seen in the electrodes is likely to be entirely from the active component. The CB electrode data used was the same as our previously reported CB electrode data¹.

Assuming a linear capacity-ratio relationship and that the PVDF is non-active, the CB contribution to the acid electrodes was determined 85 mAhg^{-1} when calculated based on the mass of the acid.

Electrode variability

Electrode formulation and processing was kept consistent across all electrode batches. However, due to method in which the reaction is taking place, i.e., a surface/slurry reaction that is unstirred and competing with solvent evaporation, the reaction is inherently difficult to control and hence variable. While it is demonstrated that the different acids undergo the reaction to different extents, it is also evident that electrodes made from an individual acid have significant variability both within the electrode, and across electrode batches due to the variability of the reaction. The reaction variability likely leads to differences in product deposition i.e., inhomogeneity, as well as differences in the nature and quantity of any side products generated.

Supplementary tables and figures

Table S1: C, O, F, Cu and N mass ratios for pristine electrodes, rounded to the nearest %.

Electrode	C%	O%	F%	Cu%	N%
CB	95 (1)	-	5 (1)	-	-
SUC	71 (2)	18 (2)	4 (1)	6 (1)	-
ASP	76 (4)	11 (3)	5 (1)	-	7 (3)
MAL	69 (2)	14 (3)	3 (1)	14 (1)	-
MEC	51 (1)	21 (1)	2 (1)	25 (2)	-
TRO	69 (1)	12 (1)	5 (1)	13 (1)	-

Table S2: C, O, N and F mass ratios for pristine aluminium-based electrodes, rounded to the nearest %, with error in brackets.

	C%	O%	N%	F%
ASP electrode	75 (6)	16 (4)	13 (5)	5 (1)
MAL electrode	82 (4)	15 (4)		3 (1)
MEC electrode	81 (1)	16 (1)		3 (1)
TRO electrode	85 (2)	7 (2)		5 (1)

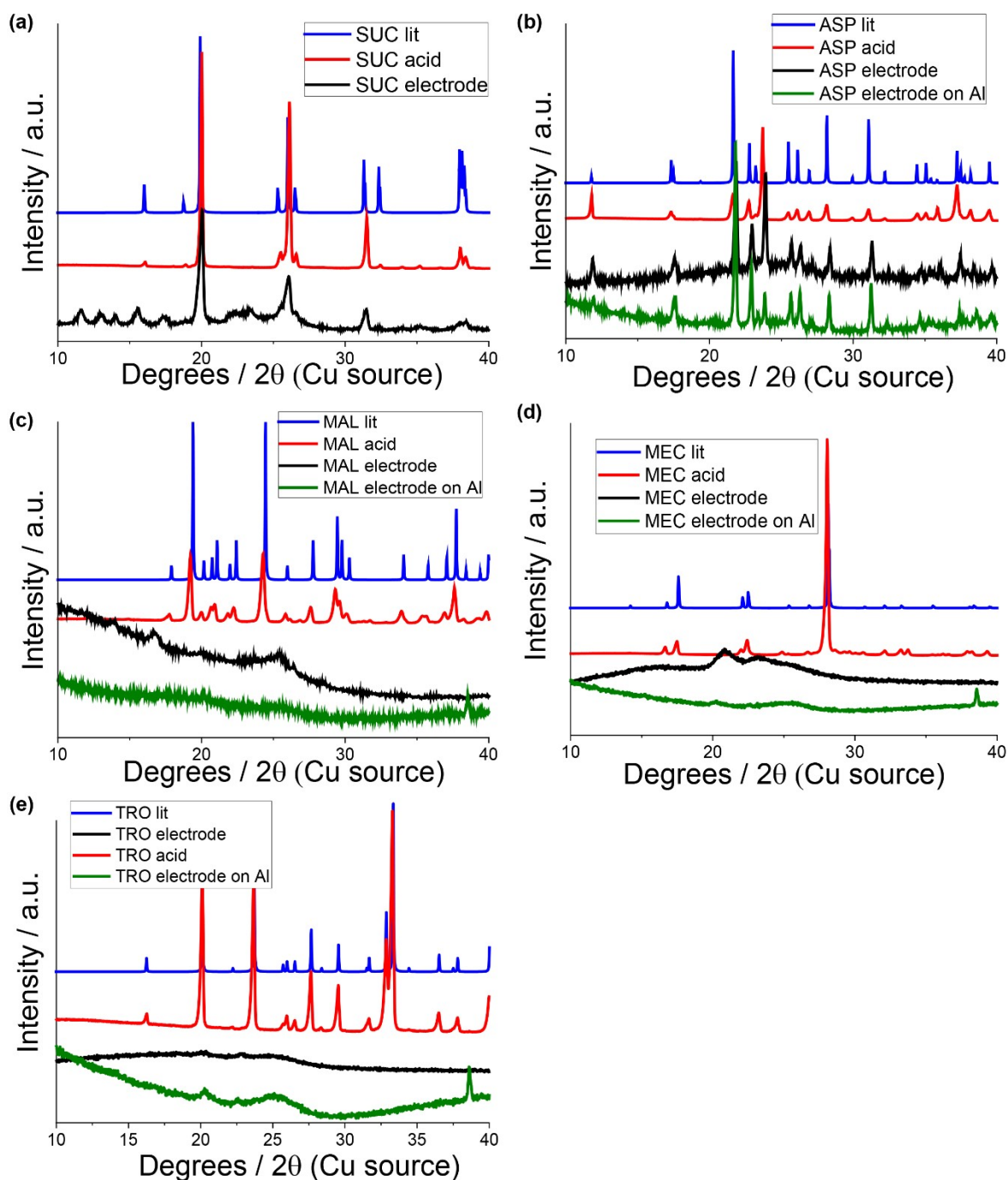
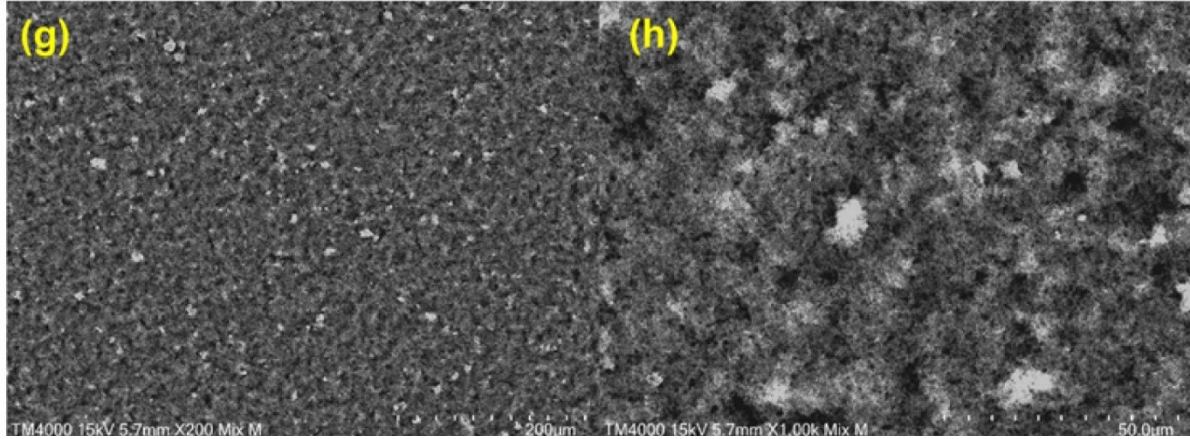
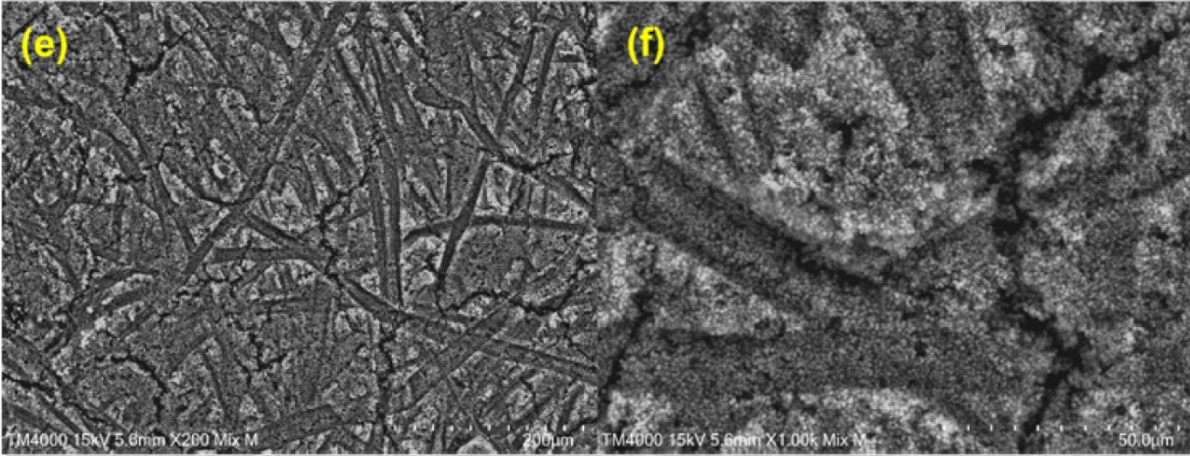
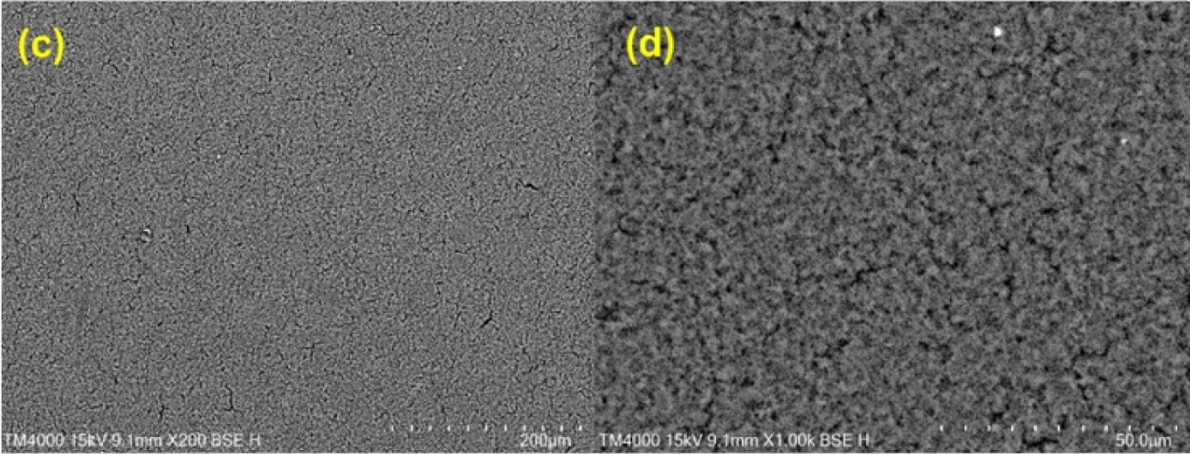
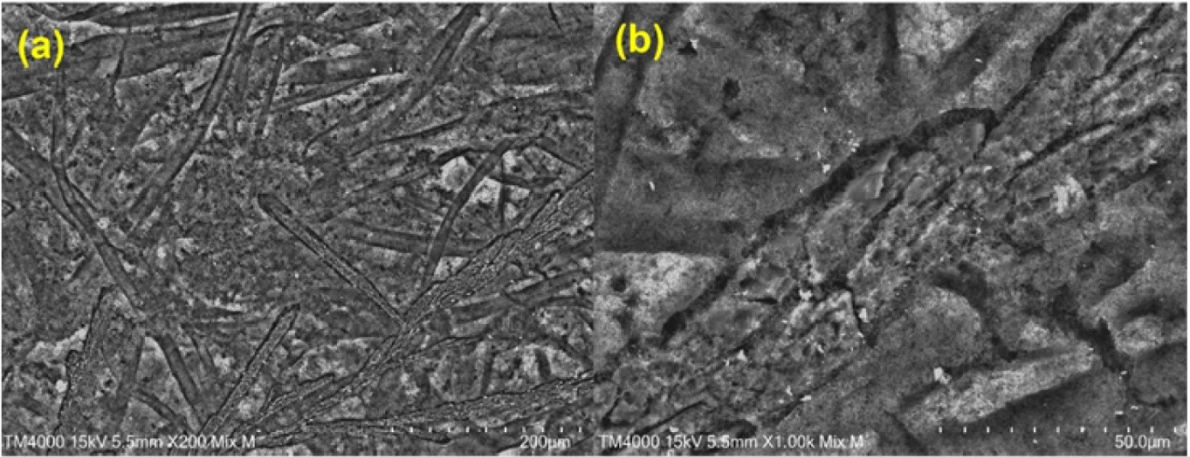


Figure S1: Comparison of XRD patterns of literature acid (blue), parent acid (red), electrode on copper (black) and electrode on aluminium (green) of (a) succinic acid², (b) aspartic acid³, (c) malic acid⁴, (d) maleic acid⁵ and (e) tartronic acid⁶ by XRD. XRD patterns multiplied by varying factors for increased visibility.



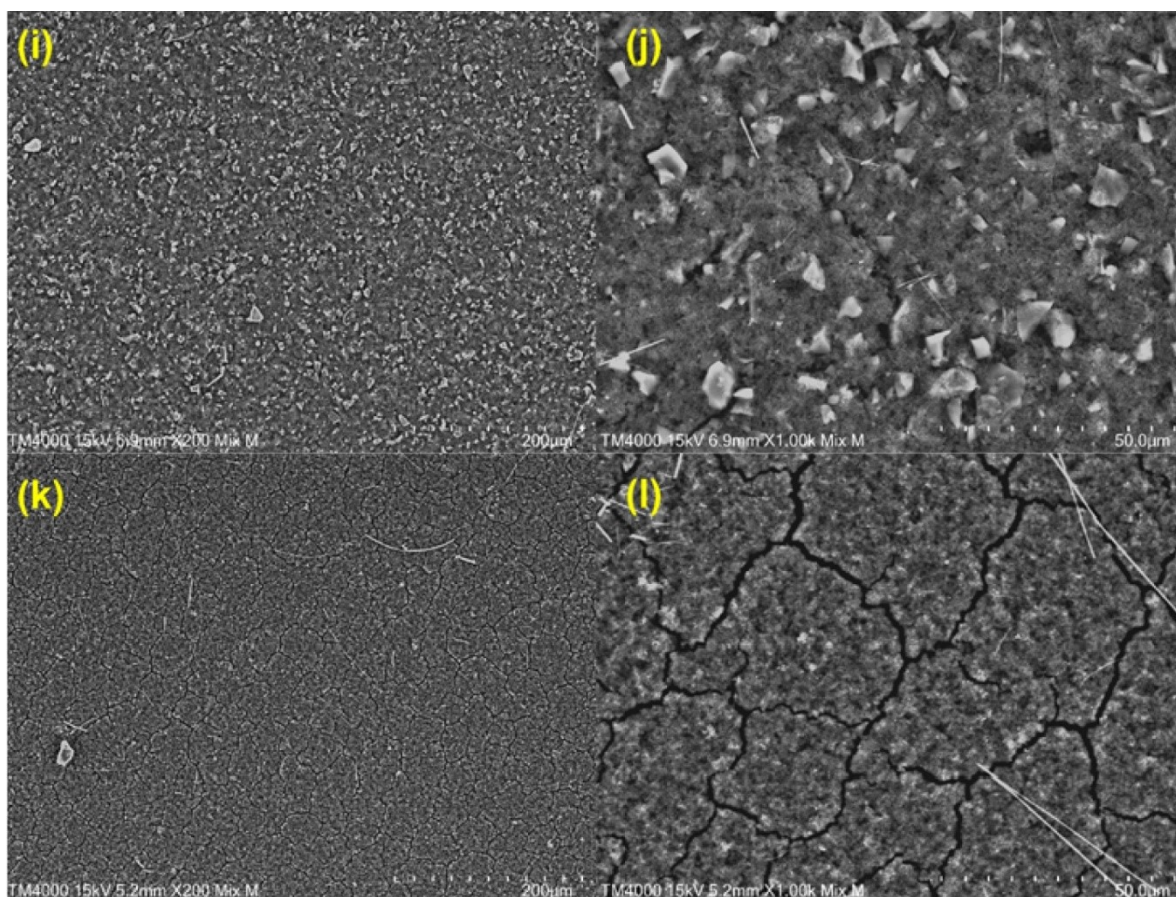


Figure S2: SEM of (a) succinic acid electrode at 200x magnification, (b) succinic acid electrode at 1000x magnification, (c) malic acid electrode at 200x magnification, (d) malic acid electrode at 1000x magnification, (e) maleic acid electrode at 200x magnification, (f) maleic acid electrode at 1000x magnification, (g) carbon black electrode at 200x magnification, (h) carbon black electrode at 1000x magnification, (i) 30x cycled aspartic acid electrode at 200x magnification and (j) 30x cycled aspartic acid electrode at 1000x magnification, (k) 30x cycled malic acid electrode at 200x magnification and (l) 30x cycled aspartic acid electrode at 1000x magnification. Cycling conducted at 50 mA g^{-1} , between 0.01 and 3 V, ending after charge to 3 V.

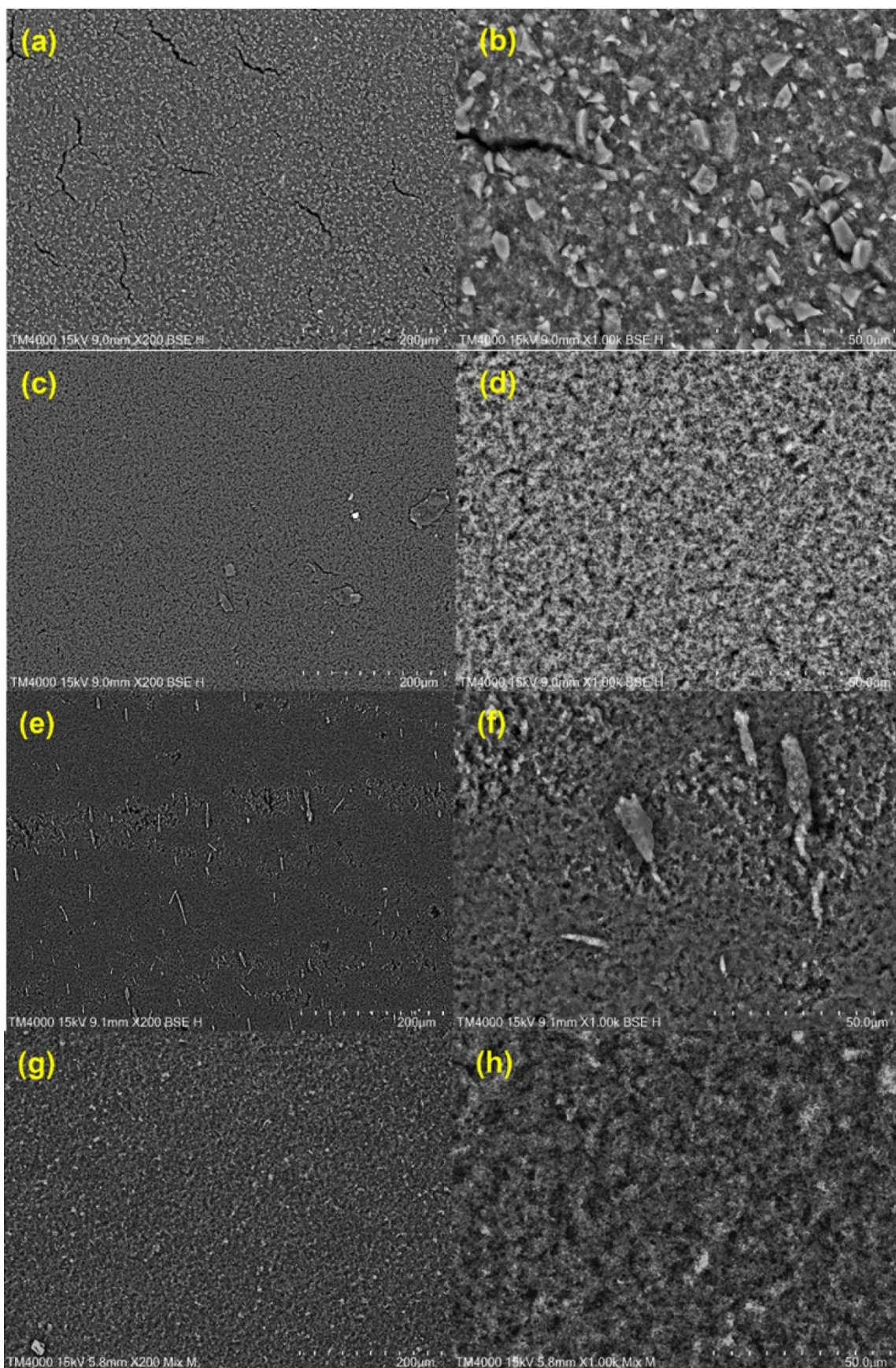


Figure S3: SEM of acid electrodes cast on aluminium substrate. (a) aspartic acid electrode at 200x magnification, (b) aspartic acid electrode at 1000x magnification, (c) malic acid electrode at 200x magnification, (d) malic acid electrode at 1000x magnification, (e) maleic acid electrode at 200x magnification, (f) maleic acid electrode at 1000x magnification, (g) tartronic acid electrode at 200x magnification, (h) tartronic electrode at 1000x magnification.

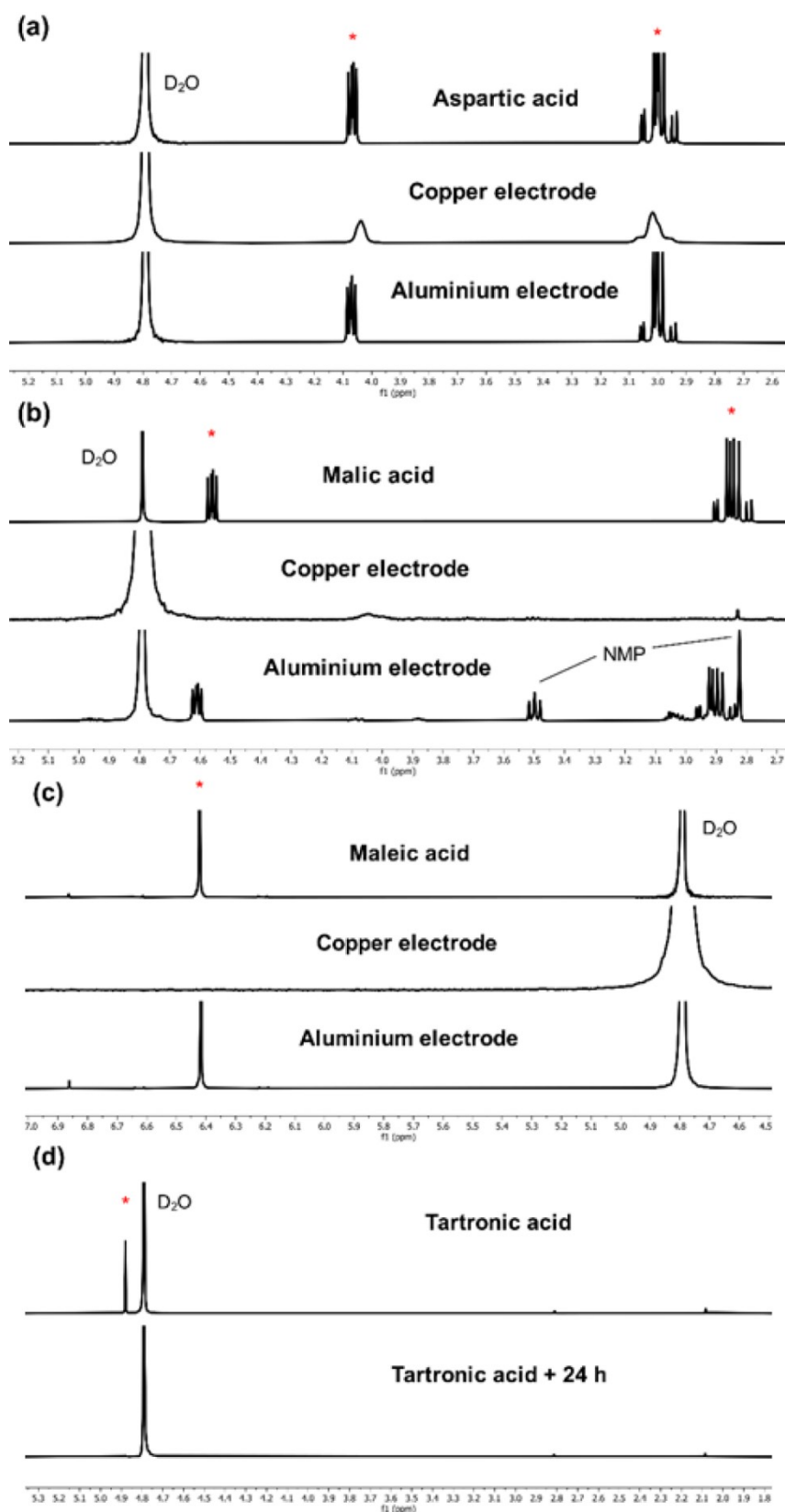
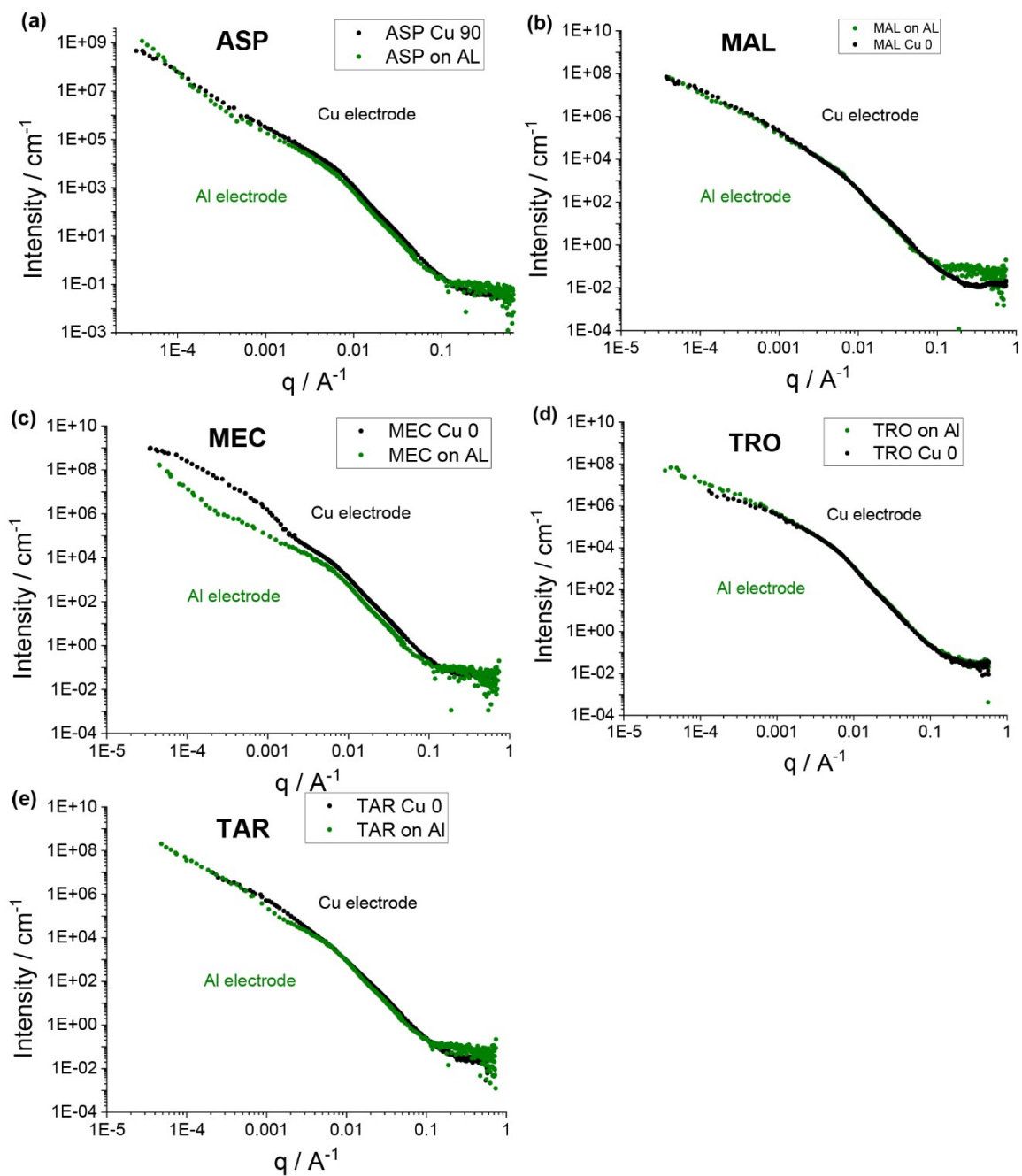


Figure S4: NMR (^1H , D_2O) of parent acid, extracted copper electrode and extracted aluminium electrode for (a) aspartic acid, (b) malic acid and (c) maleic acid. Acid peaks denoted by the red asterisk. Broadness of the aspartic acid peaks from the copper electrode likely due to concomitant extraction of Cu^{2+} species. Residual NMP peaks present (as noted) in some electrodes as a result of reduced drying to avoid sublimation of the acid. (d) NMR (^1H , D_2O) of tartronic acid (fresh) and the same sample 24 h later. Lack of tartronic acid peak demonstrates instability of the acid in water (and inefficacy of this analysis), possibly due to oxidation/hydration to mesoxalic acid⁷.



F

figure S5: Combined U/SANS data for (a) aspartic, (b) malic, (c) maleic, (d) tartronic and (e) tartaric acid electrodes, with copper (black) and aluminium (green) foil substrates.

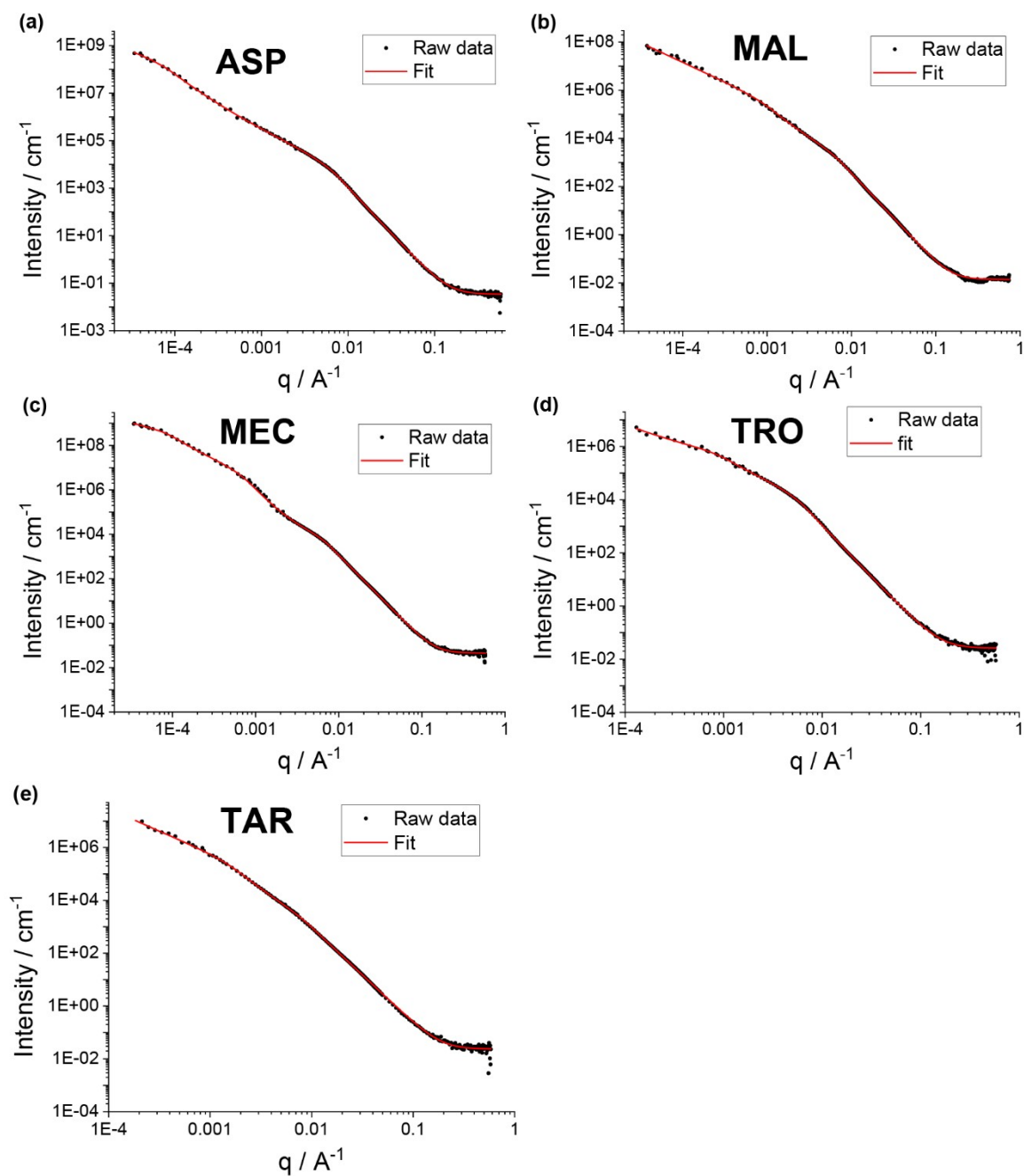


Figure S6: Raw U/SANS data (black) and fitted curves (red) for (a) aspartic acid, (b) malic acid, (c) maleic acid, (d) tartronic acid and (e) tartaric acid electrodes on a copper foil substrate. Tartaric acid raw data used is from our previous publication¹. Fitted curves were made using SASview and are a combination of Guinier-Porod and Power-law models.

Table S3: Parameters of the fitted curves for the U/SANS data for the acid on copper electrodes. “s” is the dimension variable, which relates to the shape of the scattering object, “rg” is the radius of gyration and relates the size of the scattering object, and “porod_exp” is the Porod exponent, which relates to the nature of the surface of the scattering objects. See experimental for model equations.

	scale	background	A_scale	A_rg	A_s	A_porod_exp	B_scale	B_rg	B_s	B_porod_exp			
ASP	1	0.034115	1.50	142	1.8	4.0	2152.1	13354	1.2	3.0			
MAL	1	0.014004	0.36	136	1.8	3.8	5.8681	969	1.6	3.5			
TAR	1	0.023557	0.14	87	2.0	3.6	38.994	674	1.4	3.6			
TRO	1	0.025826	12.214	201	1.4	4	5.03E+05	1891	0	3.2			
	scale	background	A_scale	A_rg	A_s	B_porod_exp	B_scale	B_rg	B_s	C_scale	C_rg	C_s	C_porod_exp
MEC	1	0.044801	133.58	216	0.9	3.8	262.68	1621	1.4	4.52E+08	19301	0.0	3.3

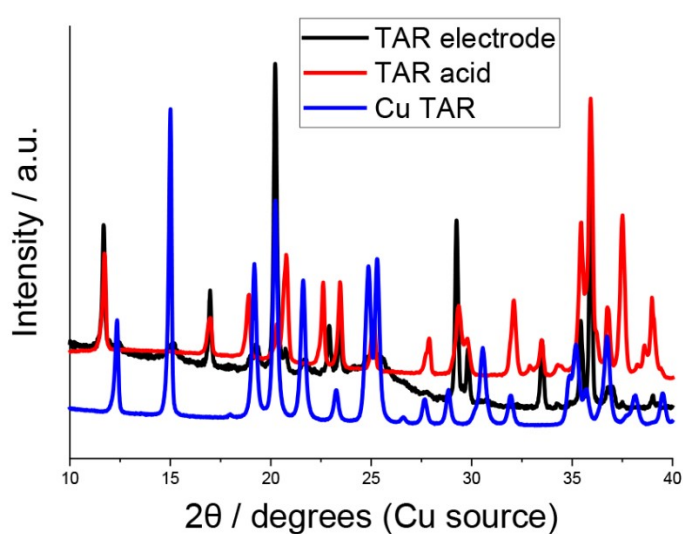


Figure S7: XRD pattern of tartaric acid electrode that was formulated using a water-based slurry (black), copper tartrate (blue) and tartaric acid (red).

	C%	O%	F%	Cu%	70 °C mass loading / mgcm ⁻¹	100 °C mass loading / mgcm ⁻¹
SUC electrode	82 (1)	5 (1)	6 (1)	4 (1)	0.8 (0.1)	1.2 (0.1)
MEC electrode	84 (1)	4 (1)	6 (1)	4 (1)	0.9 (0.1)	1.1 (0.1)

Table S4: C, O, F and mass ratios for pristine SUC and MEC electrodes that were dried at 100 °C, rounded to the nearest %, and approximate mass loadings of pristine electrodes dried at 70/100 °C, with uncertainties in brackets.

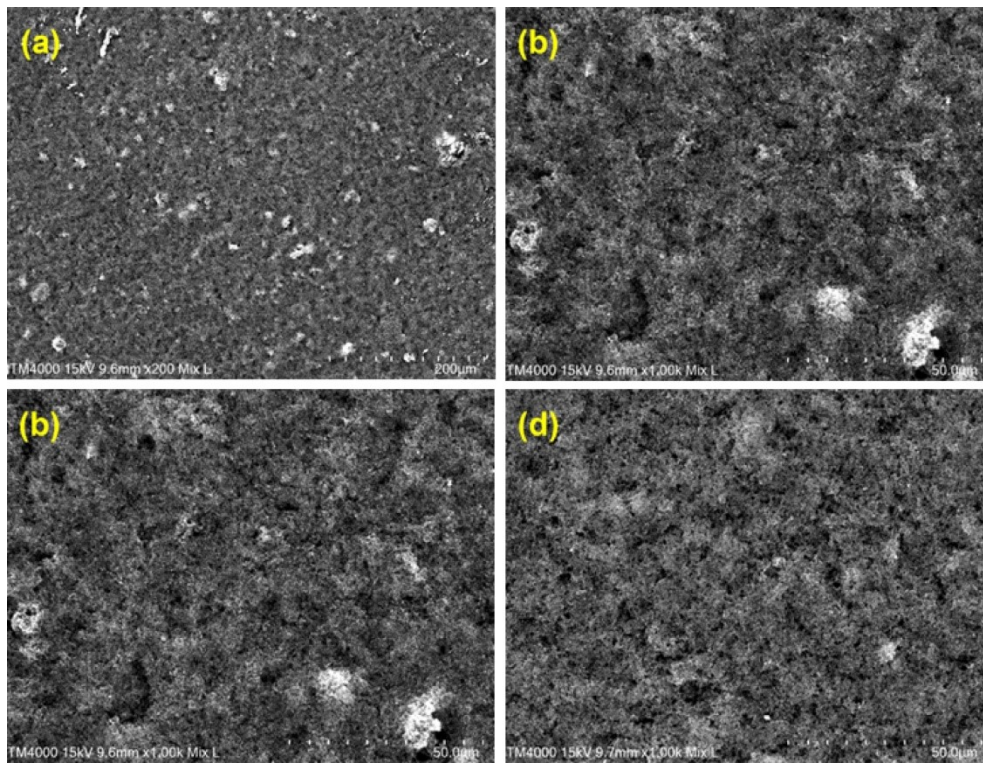


Figure S8: SEM (15 kV, 200/1000x) of SUC (a, b) and MEC (c, d) electrodes that were dried at 100 °C.

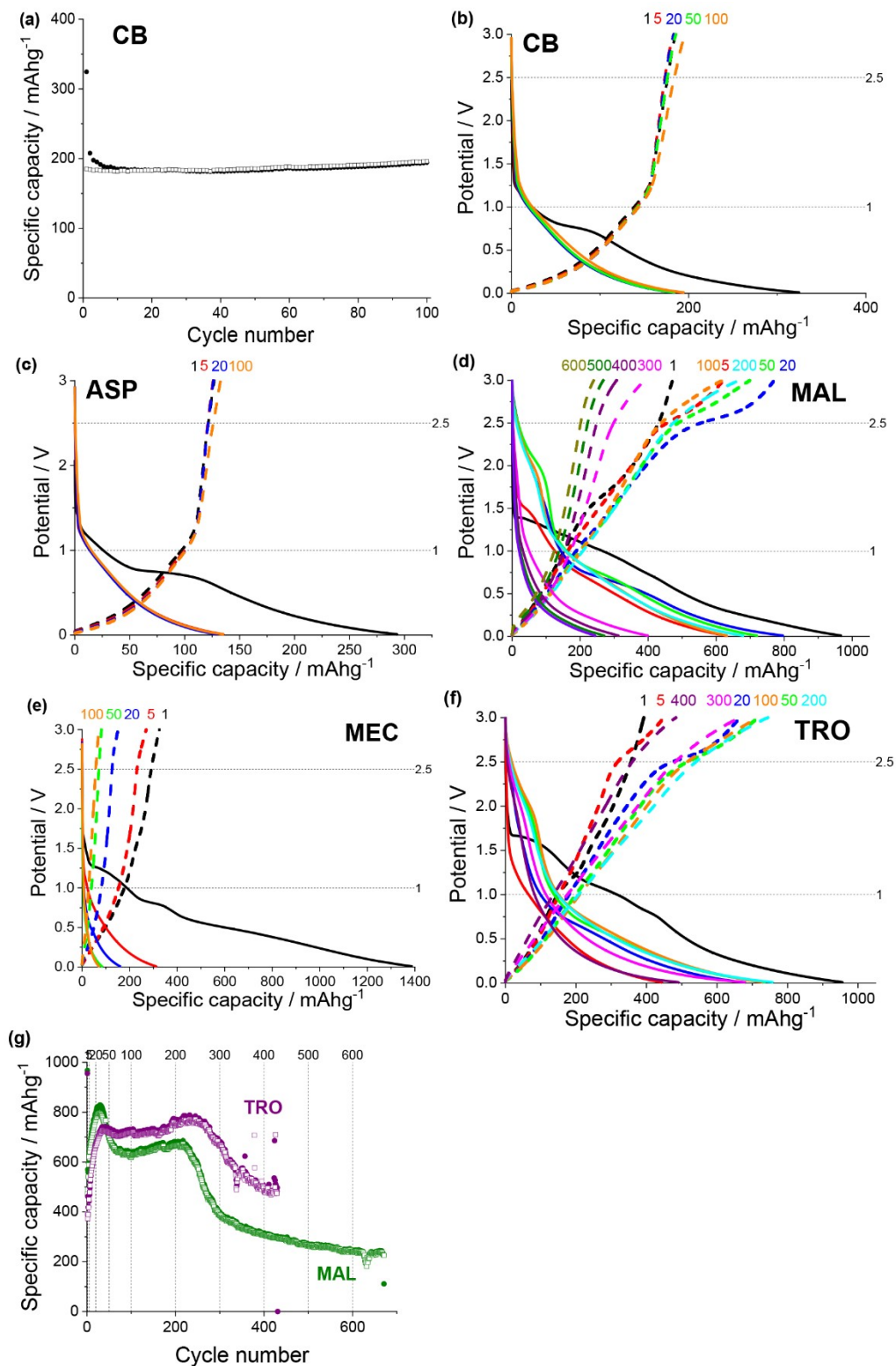


Figure S9: (a) Discharge (filled) and charge (non-filled) specific capacity vs cycle number for carbon black. (b) 1st (black), 5th (red), 20th (blue), 50th (green) and 100th (orange) discharge (solid) and charge (dashed) potential vs specific capacity curves for the carbon black electrode. Both (a) and (b) are the same data set published in our previous work¹, and are shown here for reference. (c), (d) and (e) Discharge (solid) and charge (dashed) potential vs specific capacity curves for ASP, MAL and MEC electrodes vs Li with cycling at 50 mA_g⁻¹. (f) Discharge (solid) and charge (dashed) potential vs specific capacity curves for TRO electrodes vs Li with cycling at 50 mA_g⁻¹. (g) Discharge (filled) and charge (non-filled) specific capacity vs cycle number for MAL (green) and TRO (purple) electrodes versus Li. Cycling at 50 mA_g⁻¹ between 0.01 and 3 V. Dashed lines indicate cycles displayed in (d) and (f).

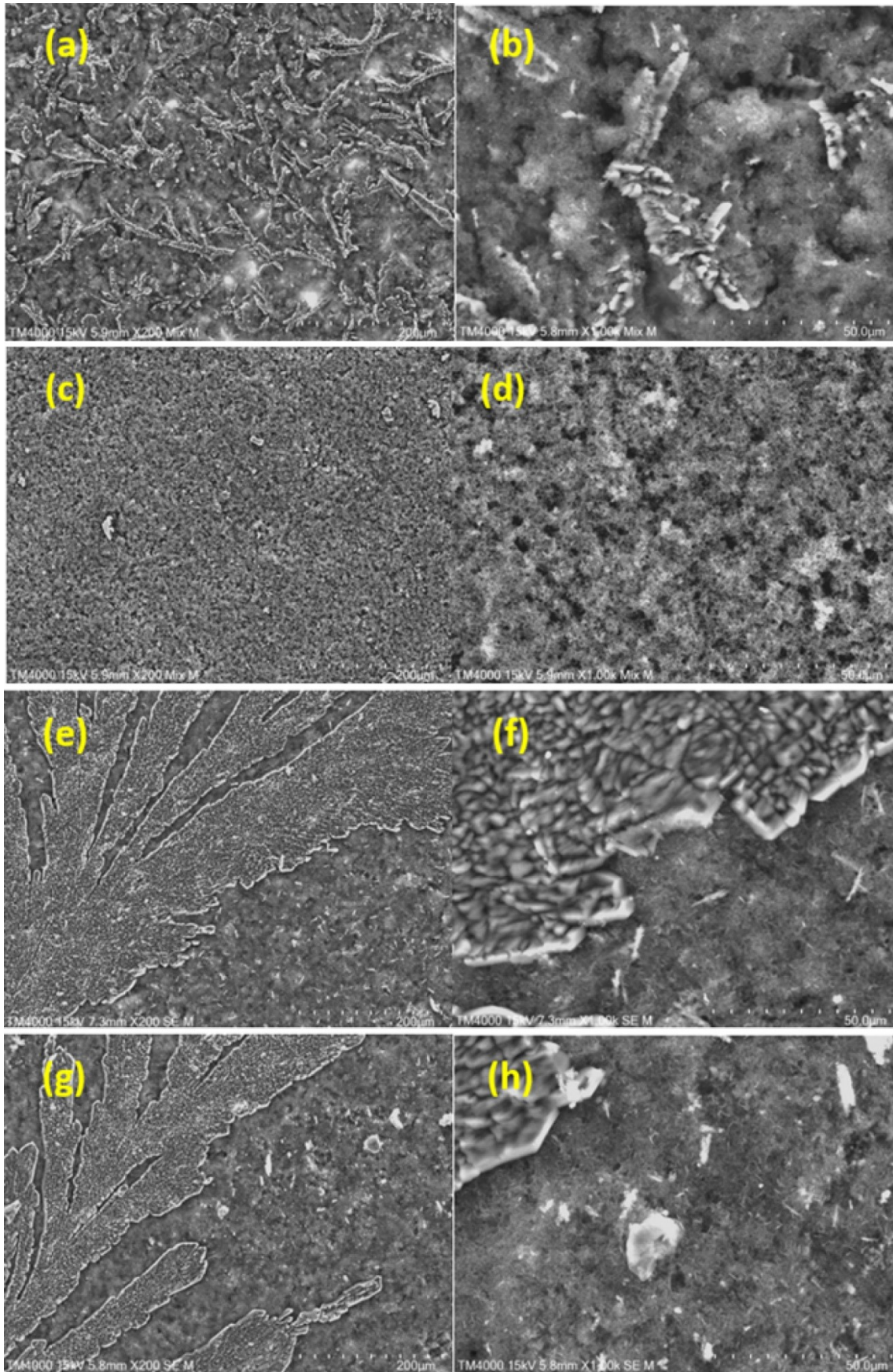


Figure S10: SEM (200x:left and 1000x:right) of SUC electrodes made with $x\%$ NMP and $1-x\%$ MeOH. (a) and (b) 0%, (c) and (d) 50%, (e) and (f) 60% and (g) and (h) 70%.

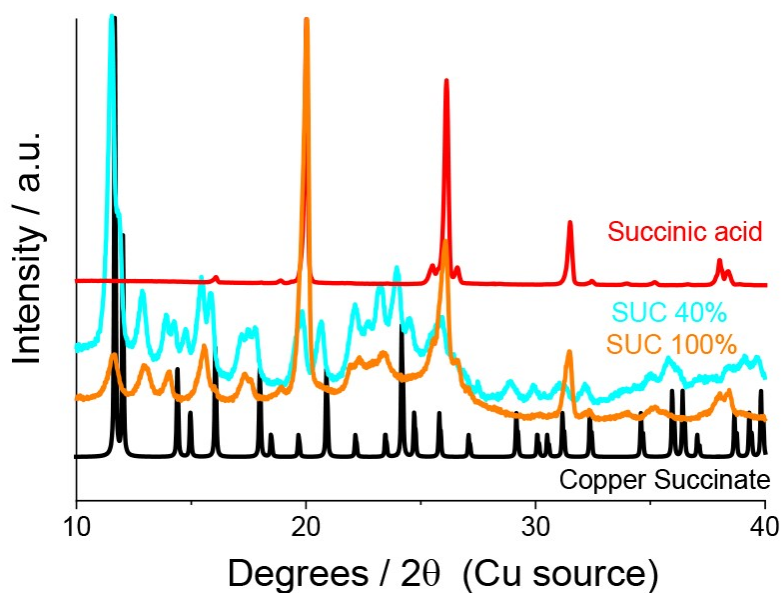


Figure S11: XRD of succinic acid (red), copper succinate⁸(black), SUC 40% (cyan) and SUC 100% (orange) electrodes. SUC electrodes made with X% NMP and 1-X% MeOH.

1. Teusner, M.; Mittal, U.; Lessio, M.; Johannessen, B.; Mata, J.; Sharma, N., Formulation and mechanism of copper tartrate - an anode material for lithium-ion batteries - under review. 2022.
2. El Moussaoui, A.; Chauvet, A.; Masse, J., Etude des interactions a l'etat solide du nordazepam III-polyoxyethylene glycol 6000 et nordazepam III-acide succinique. *Journal of Thermal Analysis* **1993**, 39 (3), 373-392.
3. Derissen, J. L.; Endeman, H. J.; Peerdeman, A. F., The crystal and molecular structure of l-aspartic acid. *Acta Crystallographica Section B* **1968**, 24 (10), 1349-1354.
4. van der Sluis, P.; Kroon, J., Structure of (-)-malic acid. *Acta Crystallographica Section C* **1989**, 45 (9), 1406-1408.
5. Shahat, M., The crystal and molecular structure of maleic acid. *Acta Crystallographica* **1952**, 5 (6), 763-768.
6. van Eijck, B. P.; Kanters, J. A.; Kroon, J., The crystal structure of tartronic acid. *Acta Crystallographica* **1965**, 19 (3), 435-439.
7. Fordham, P.; Besson, M.; Gallezot, P., Catalytic oxidation with air of tartronic acid to mesoxalic acid on bismuth-promoted platinum. *Catalysis Letters* **1997**, 46 (3), 195-199.
8. Das, S.; Srivastava, V. C., Synthesis and characterization of copper succinate and copper oxide nanoparticles by electrochemical treatment: Optimization by Taguchi robust analysis. *The Canadian Journal of Chemical Engineering* **2016**, 94 (7), 1322-1327.